Phase Error Compensation Technique for Improved Synthetic Aperture Radar Performance

Dale C. Griffith

Radar data contain phase errors whose sources include uncompensated platform motion and transmitter and receiver phase errors. Achieving theoretical resolution from a pulse compression system requires a method to minimize those phase errors. This article discusses a method of estimating and correcting phase errors in synthetic aperture radar data. The method requires that one or more stationary point targets be included in the data. The phase history of each reference target is estimated for the period in which the target is in the view of the radar. The phase error, computed as the deviation from the theoretical phase function, is estimated and removed from the raw data. Unfortunately, conventional continuous phase measurement requires high signal-to-noise ratio. To increase the effective signal-to-noise ratio of the raw reference target data, the targets are extracted after matched filtering, and the resulting data are inverse matched filtered. In one test data set, this phase correction method improved the synthetic aperture radar image resolution by 50%.
(Keywords: Inverse filtering, Phase error correction, Synthetic aperture radar.)

INTRODUCTION

Since 1983, the Submarine Technology Department has been developing and applying a synthetic aperture radar (SAR) processor. This system can process data from many SAR systems: Seasat, SIR-A (shuttle imaging radar), SIR-B, Jet Propulsion Lab DC-8 SAR, Environmental Research Institute of Michigan CV580 SAR, Naval Air Defense Center (NADC) P-3 SAR, and Canadian Centre for Remote Sensing C-IRIS SAR. The processor was adapted to three different computer systems: DEC VAX 785 with FPS-164 array processor, DEC uVAX II with numerix array processor, and DEC uVAX II.

Over the processor's history, the resolution of SAR images improved 10-fold because of the increased bandwidth of the SAR systems. The improved resolution necessitated improving SAR processing. The initial processor was created to process data from Seasat, a relatively low resolution satellite system.[1] The final

incarnation could process data from the NADC P-3 SAR, a high-resolution airborne system. Both the higher resolution and the airborne platform make processing the data more difficult. Higher resolution requires the processor to have greater precision. Unlike satellites, airborne systems, such as airplanes, are buffeted by wind and turbulence, which cause them to stray slightly from the desired path, a straight line, during the image formation aperture. Nonlinear motion is accounted for by adding a motion-compensation algorithm into the processing chain.

One approach to compensate for platform motion is to estimate and then correct for the phase errors introduced by the motion. Phase error correction algorithms include map drift,[2] phase difference, phase gradient algorithm,[3] spatial correlation algorithm, prominent point processing (PPP),[4] and inverse filtering.[3] Map drift and phase difference form multiple subsets of data and correlate the corresponding images to form a polynomial estimate of the phase error, where the order of the polynomial equals the number of subsets. The spatial correlation and phase gradient algorithms are adaptations of the shift-and-add algorithm, from speckle interferometry within astronomy, where data from each range form a low SNR estimate of the phase error. The estimates for each range are combined in a least-squares sense to estimate the phase error. In PPP, an operator adjusts the raw data so that strong targets match their expected response. Inverse filtering infers the phase error by deconvolving the blur associated with a strong target from the response of the target. All of these methods require some structure within the scene. PPP and inverse filtering are not automatic and can only be applied to scenes containing strong, stationary point targets.

This article discusses an algorithm to measure a radar's phase error, using a combination of the inverse filtering phase estimation method and PPP. The algorithm can be viewed as a stripmap SAR implementation of either PPP or inverse filtering. (A stripmap is an image of a long narrow area of terrain parallel to the flight path.) The phase error estimates have been used to correct the SAR image. The resulting image quality improvements are also discussed.

BACKGROUND

SAR is a method of obtaining high-resolution radar backscatter information. It differs from conventional radar in that it achieves much greater azimuth resolution from a comparably sized antenna and the azimuth resolution has no range dependence. SAR systems produce images, three-dimensional representations, where the image intensity expresses the reflectivity of the scene as a function of the range and azimuth location.

SAR achieves high resolution by forming a very long virtual antenna array. The virtual array is created using a single array element and moving that element to the location of each synthetic array element to collect the data for that synthetic element. This is typically accomplished by placing the real element on an airplane or satellite and collecting data while the platform is moving.

The SAR image is created by beamforming the data from the array. High-resolution SAR beamforming occurs in the near field. However, the elements of the virtual array are directional so the array can only form a beam in a single direction. For the purpose of discussion, this beam is assumed to be pointed broadside to the flight path. The array dimensions are determined by the flight and radar parameters. One notable feature of SAR is that the resolution is independent of range. This is quite an advantage over conventional radars whose resolutions are determined by the antenna beamwidth, which is inversely proportional to the antenna size and results in a cross-beam (azimuthal) resolution dependence on range. The constant azimuthal resolution of a SAR is achieved by synthesizing a longer array for greater range viewing, in contrast to a real array radar whose number of elements is fixed, thereby causing the antenna beamwidth to be fixed and the azimuth resolution to degrade with range. The image has dimensions of range and azimuth (cross-range). High-range resolution is typically achieved with a long-pulse, high-bandwidth waveform. Processing in the range direction compresses the data to the equivalent of a short-duration impulsive waveform.

The theoretical response of an ideal scatterer is $e^{-j2\pi\phi(t)}$, where $\phi(t)$ is the phase of the radar returns, measured in units of 2π radians. Assuming no phase shift on reflection, the phase of the radar returns is the range in wavelengths of the radar carrier. Assuming the plane flies a straight path, the range from the plane to a target is

$$R(t) = \sqrt{R_0^2 + v^2 t^2} \, , \qquad (1)$$

where t is time, R_0 is the range at the closest point of approach, and v is the plane's speed as diagrammed in Fig. 1. However, the phase uses the round trip distance because the radar pulse must travel to the target and then return to the radar. The phase is typically approximated with a binomial series, such as the following:
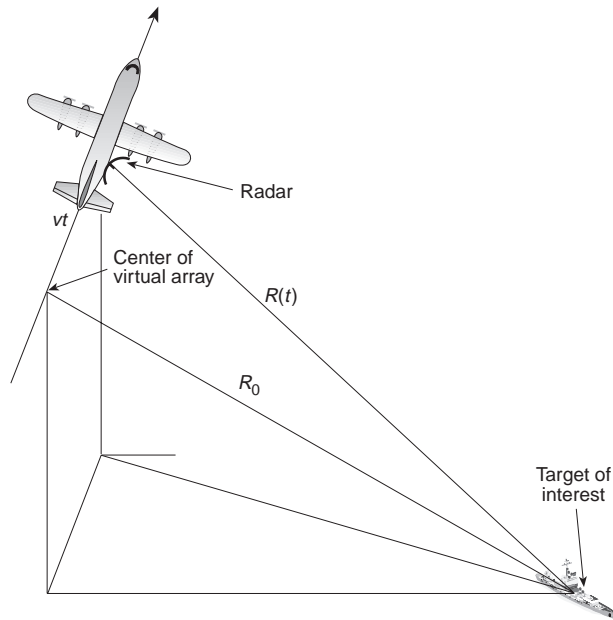
Figure 1. SAR data collection geometry.

Figure 2. Example of theoretical target response (red curve) and target response with phase error (blue curve). The peak response is degraded and shifted.

$$\phi(t) = \frac{2R(t)}{\lambda}$$
$$\approx \frac{2}{\lambda}\sqrt{R_0^2 + v^2 t^2}$$
$$= \frac{2R_0}{\lambda} + \frac{v^2 t^2}{\lambda R_0} \qquad (2)$$
$$= \frac{2R_0}{\lambda} + \frac{x^2}{\lambda R_0},$$

where λ is the radar carrier wavelength and x is the cross-range distance from the center of the array. For example, the phase function of a target at 7.5 km, as viewed by an L-band ($\lambda = 24$ cm) radar traveling at 125 m/s, is a hyperbola whose amplitude changes from approximately 28,000° to 0° and back to 28,000° in 6 s. Traditional near-field beamforming applies a phase shift of

$$e^{j2\pi\phi(t)} = e^{j2\pi\frac{x^2}{\lambda R_0}} \qquad (3)$$
$$= h(x),$$

which will align the data and produce a well-defined image. Processing an ideal target generates a sin x/x function with a width of 0.007 s for the preceding parameters as shown in Fig. 2.
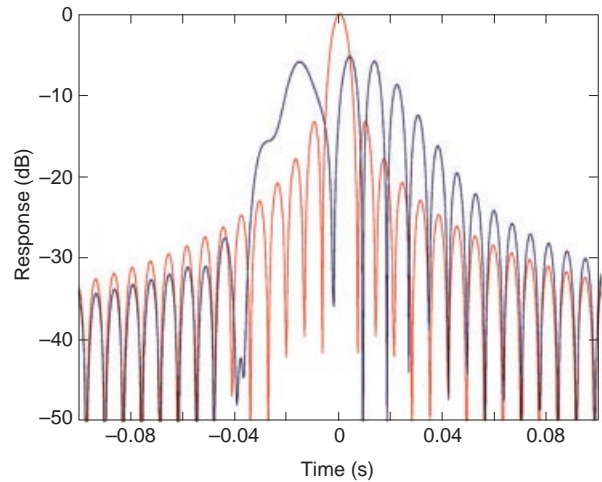
If phase errors are introduced, the azimuth beamforming gain is reduced. The phase errors appear in the image as a loss of resolution, a decrease in dynamic range, and an increase in noise. For example, if a phase error (a sine wave with a 6-s period and 180° amplitude, corresponding to a 12-cm cross-track deviation from the desired flight path) is added to the ideal phase signal, the response, also shown in Fig. 2, is severely degraded, with the peak reduced by 5 dB. A complete explanation of the effect of phase errors on SAR imagery is available.[5] The performance sensitvity to small phase errors necessitates measuring and correcting the phase fidelity of the radar.

A potential source of phase errors for an airborne SAR is radar motion off the linear path assumed by the beamforming algorithm. Unfortunately, the tolerance associated with a straight path is very stringent: the phase center of the radar antenna must stay within $\lambda/8$ (3 cm at L-band) of a perfectly straight line, and the radar pulses must occur within $\lambda/8$ of being evenly spaced for the duration of the synthetic aperture (typically 1 to 10 s) to achieve theoretical resolution. However, a phase error correction algorithm can restore theoretical resolution.

PHASE MEASUREMENT

Traditional beamforming shifts the data from each element of the antenna array to align the response of a target in the data. Aligning the response of a target in the data makes the data add coherently and constructively. The amount of shift is determined theoretically. The concept of PPP is to use the response of a strong target to improve the alignment. In PPP the

location of the peak response of a "prominent point" is measured. The amount of shift is that which is required to make the data from each element align. However, two difficulties exist in PPP. First, it requires a high single-pulse signal-to-noise ratio (SNR), i.e., the target must be detected in the unprocessed data from each array element. Second, the data must be aligned to within $\lambda/8$, which is much finer than the range resolution of the data. Therefore, to achieve the required precision, the alignment must use the phase of the target data.

However, the target's response in the unprocessed data is generally obscured by the surrounding area's response and can be difficult or impossible to isolate. Each sample represents not just the target but a superposition of responses from many scatterers in the physical radar beam. The physical radar beam is typically 1000 times larger, in the azimuth direction, than a SAR image cell. In actual data, the target SNR is not generally sufficient to perform PPP. However, with the method to be described here, it is possible to isolate the data associated with a target.

SAR processing collects the entire response of a target in a small spatial region and separates the target's response from nearby background features. However, the target's phase history is not available in the SAR image. Fortunately, the original data can be restored by reversing the processing. SAR processing is analogous to beamforming but can also be performed by pulse compression. A flow diagram of this type of processing is shown in Fig. 3. Mathematically, the image is

$$s(x, y) = \text{IFFT}[G(u, y)H(u)], \qquad (4)$$

where $s(x,y)$ is the (complex) SAR image, IFFT is the inverse fast Fourier transform, $G(u,y)$ is the azimuth spectrum of the range-compressed data, $H(u)$ is the compression filter spectrum, x is the cross-range position, y is the range position, and u is the cross-range frequency. Reversing this expression, the phase history can be calculated by inverse filtering the SAR image, given by

$$G(u, y) = \frac{S(u, y)}{H(u)}$$
$$g(x, y) = \text{IFFT}\left[\frac{S(u, y)}{H(u)}\right], \qquad (5)$$

where $g(x,y)$ is the range compressed data and $S(u,y)$ is the azimuth spectrum of the SAR image. Using the last expression, the phase history associated with a target can be obtained by first processing in azimuth,

then windowing away all nondesired data, and finally reversing the processing, i.e.,

$$\hat{g}(x, y) = \text{IFFT}\left[\frac{\hat{S}(u, y)}{H(u)}\right], \qquad (6)$$

where $\hat{S}(u, y)$ is the spectrum of the data near the target from the image and $\hat{g}(x, y)$ is the target's phase history. The resulting phase history has a much higher SNR than in the original data. A flow diagram of the target isolation processing is also shown in Fig. 3.

After target isolation, the target will typically dominate the data from each array element, that is, the target should be the peak signal level. The location of the peaks is a coarse estimate of the target's phase history because
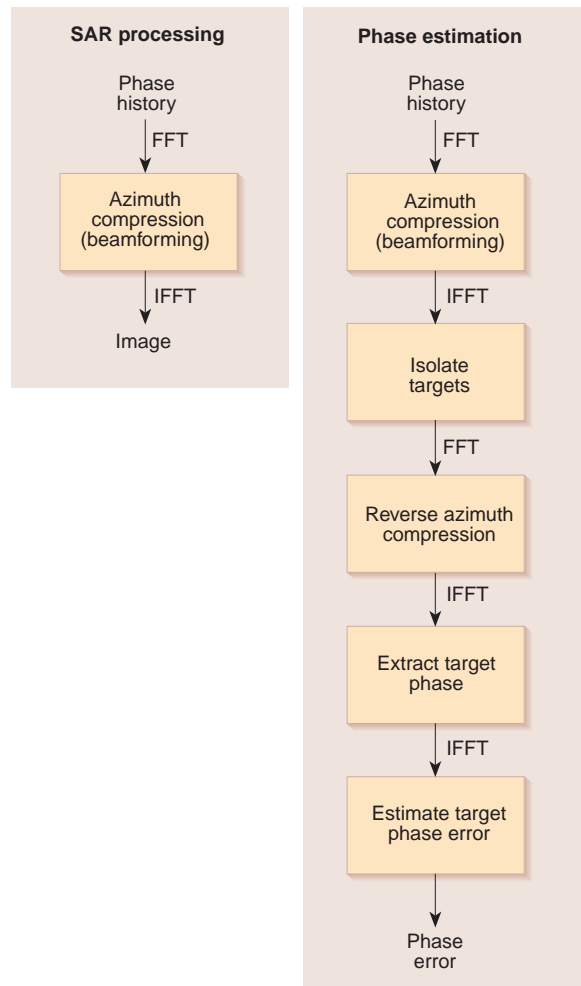

Figure 3. Processing flow for standard SAR processing and SAR processing with phase error estimation.

$$\phi(t) = \frac{2R(t)}{\lambda}. \qquad (7)$$

The target's measured phase history is

$$\hat{\phi}(t) = \arg \hat{g}(t)$$
$$= \arg \hat{g}\left(\frac{x}{v}\right), \qquad (8)$$

where $\hat{\phi}(t)$ is the target phase as a function of time.

The phase error ϕ_e is the difference between the measured phase function and the theoretical phase function. A least-squares-fit parabola is a good estimate of the theoretical phase function. The phase error is removed by multiplying the original data by $e^{j2\pi\hat{\phi}_e(t)}$, as follows:

$$g_c(x, y) = g(x, y)e^{j2\pi\hat{\phi}_e\left(\frac{x}{v}\right)}, \qquad (9)$$

where c denotes the corrected phase history.

EFFECT OF PHASE ERROR

The phase error was measured for the NADC P-3 SAR pass on 4 June 1990 at 2034 UTC. The scene was a reflector array on Andros Island. The reflector array contained 12 trihedral corner reflectors, 9 of which were visible in the standard SAR image. The error functions for all targets are shown in Fig. 4. Note that all the targets have the same error as a function of time.

The image was processed normally and then processed again with the raw data multiplied by $e^{j2\pi\hat{\phi}_e(t)}$. The uncorrected image is shown in Fig. 5, and the phase-adjusted image is shown in Fig. 6. The point targets are all much sharper in the corrected image. In fact, three additional reflectors are visible at the end of the reflector array. The clutter at the right side of the image just above and below the dark area is better resolved, as well.
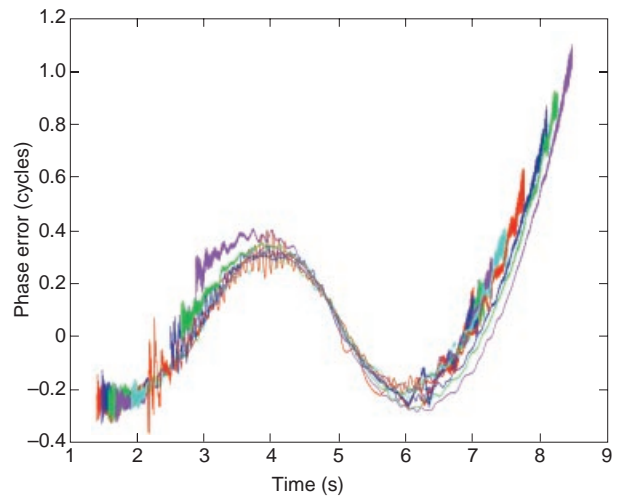

Figure 4. Phase error as a function of time measured in actual SAR data for all nine reflectors. The data show consistent phase errors for all reflectors. The average phase error is of sufficient magnitude to induce significant image artifacts.

Figure 7 shows an example mesh plot of a target for both images, again showing an improvement in the azimuth response of the point targets. The range response is largely unchanged, as expected. The azimuth response is improved by the phase correction. The original processing showed a broad azimuth target width, whereas the corrected data have a

Figure 5. The uncorrected SAR image. The image contains 12 reference radar reflectors, only 9 of which are clearly visible. The visible targets show significant azimuthal blurring.

Figure 6. The corrected SAR image. The image contains 12 reference radar reflectors. Note that the targets are well defined. The clutter in the lower right-hand corner is well defined, also.
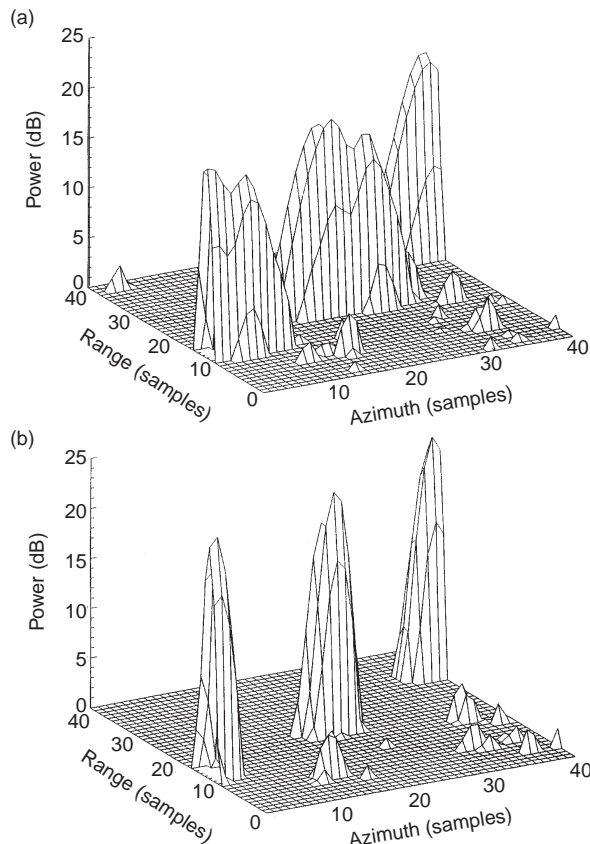

Figure 7. Mesh plot of target 2: (a) uncorrected and (b) corrected. Parts of targets 1 and 3 are also visible. The corrected image shows much better defined targets.

narrow, well-defined azimuth target response.

To quantify the processing improvement, two standard signal processing measures were chosen: integrated sidelobe ratio (ISLR) and 6-dB width. Before measurement, the target's azimuth response was interpolated by 4 using a sin x/x function. For this analysis, the ISLR is the ratio of the area of the mainlobe to the area of the sidelobes, where the mainlobe is the region between the 6-dB down points. The sidelobes are the regions outside the mainlobe and within a 128-point window, which is a large enough region to ensure that all the sidelobe energy is included. The ISLRs for all nine targets are listed in Table 1. Every target's ISLR is significantly improved. On average, the ISLRs showed a 5-dB improvement after phase correction. The 6-dB widths are also listed in Table 1. The phase correction also significantly improved the 6-dB width for every target. On average, the 6-dB width showed a factor of improvement of 2.0.

CONCLUSION

A phase error measurement and compensation method for SAR was presented. The technique uses a phase estimate of a reference target and uses inverse filtering to extract the reference target with high SNR. An example scene contained an error that degraded the point target response and consequently the image quality of the radar by 5 dB. By measuring and removing the radar phase error, the image was processed to the theoretical resolution.

REFERENCES

[1] McDonough, R. N., Raff, B. E., and Kerr, J. L., "Image Formation from Spaceborne Synthetic Aperture Radar Signals," *Johns Hopkins APL Tech. Dig.* **6**(4), 300–312 (1985).
[2] Curlander, J. C., and McDonough, R. N., *Synthetic Aperture Radar: Systems and Signal Processing*, John Wiley and Sons, New York (1991).
[3] Jakowitz, C. V., Jr., Wahl, D. E., Eichel, P. H., Ghiglia, D. C., and Thompson, P. A., *Spotlight-Mode Synthetic Aperture Radar: A Signal Processing Approach*, Kluwer Academic Publishers, Boston (1996).
[4] Carrara, W. G., Goodman, R. S., and Majewski, R. M., *Spotlight Synthetic Aperture Radar: Signal Processing Algorithms*, Artech House, Boston (1995).
[5] Younkins, L. T., *The Effects of Phase Error on Azimuth Compression in Synthetic Aperture Radar*, STS-88-176, JHU/APL, Laurel, MD (2 Aug 1988).

Table 1. Point target response comparison between the standard processing and the phase-adjusted processing, which shows that the phase adjustment improved the target SNR by 5 dB and the resolution by a factor of 2.0.

Target	Integrated sidelobe ratio (dB)		6-dB width (m)	
	Standard	Phase adjusted	Standard	Phase adjusted
1	2.1	9.6	5.7	2.0
2	2.5	10.0	5.5	2.0
3	5.7	9.7	3.1	2.0
4	4.3	9.7	3.7	2.0
5	5.5	9.8	3.4	2.0
6	5.8	9.8	3.1	2.0
7	7.0	9.8	3.2	2.0
8	5.6	10.2	3.4	2.0
9	4.8	10.8	4.5	2.0
Average	4.8	9.9	4.0	2.0

THE AUTHOR

DALE C. GRIFFITH received B.S. and M.S. degrees in electrical engineering from Michigan State University. His work has focused on signal processing as applied to SAR, sonar, and conventional radar. He is a member of the Submarine Technology Department's Signal and Information Processing Group. His e-mail address is Dale.Griffith@jhuapl.edu.